Laser-induced-fluorescence characterization of velocity shear in a magnetized plasma column produced by a segmented, Q-machine source

doi: 10.1063/1.1925616

Laser-induced-fluorescence characterization of velocity shear in a magnetized plasma column produced by a segmented, *Q*-machine source

E. W. Reynolds
Physics Department, West Virginia University, Morgantown, West Virginia 26506-6315

T. Kaneko
Graduate School of Engineering, Tohoku University, Sendai 980-8579, Japan

M. E. Koepke
Physics Department, West Virginia University, Morgantown, West Virginia 26506-6315

R. Hatakeyama
Graduate School of Engineering, Tohoku University, Sendai 980-8579, Japan

(Received 12 January 2005; accepted 8 April 2005; published online 20 June 2005)

Control over the radial profile of one component of ion drift speed $\boldsymbol{U}$, either perpendicular or parallel to the magnetic field, is demonstrated in the magnetized plasma column for two configurations of a double-ended *Q* machine in which one of the hot plates is segmented into a central disk and two concentric annuli. Each hot plate can be heated to ~1800 °C, and the segmented hot plate is bombarded with barium vapor, resulting in quasineutral, magnetized, barium-ion plasma. Since the electric potential in the plasma magnetically maps to the segments, the radial profile of plasma potential, and hence the $E \times B$ flow, can be made inhomogeneous. This configuration is referred to as the perpendicular configuration. A negatively biased, cross-sectional mesh, inserted between the two ends of the plasma column, reflects electrons from each source causing the radial profile of potential on the nonsegmented source side of the mesh to become uniform. In traversing the mesh sheath from the segmented source side, where the radial potential profile is inhomogeneous, to the nonsegmented source side, where the radial potential profile is homogeneous, the ions experience an axial acceleration that has an inhomogeneous radial profile. This configuration with the mesh is referred to as the parallel configuration. Laser-induced-fluorescence is used to measure the ion-velocity-distribution function on the nonsegmented-source side with and without the mesh inserted. Measurements show that the above configurations result in ion temperature anisotropy, $1 < (T_\perp / T_\parallel) < 5$, and radially nonuniform ion flows with a maximum in the shear profile $(dU_\perp / dx)_{\max}$ as large as $0.6\,\Omega_i$ and $(dU_\parallel / dx)_{\max}$ as large as $0.17\,\Omega_i$ where Ω_i is the ion gyrofrequency. © *2005 American Institute of Physics*. [DOI: 10.1063/1.1925616]

I. INTRODUCTION

Q machines[1] have played an important role in the experimental study of low-frequency ($\omega \ll \Omega_e$, where Ω_e is the electron gyrofrequency) electrostatic ion waves in low-temperature, magnetized plasmas. The *Q*-machine source[1–3] has the benefit of producing alkali plasma that is both quiescent (which simplifies detection of low-amplitude waves) and collisionless (a feature applicable to the upper ionosphere and magnetosphere[4]). Theoretical predictions regarding the influence of sheared ion flows on the excitation and propagation of electrostatic plasma waves[5–8] have motivated experiments using several *Q*-machine configurations,[10–16] in which inhomogeneous ion flow is a key feature. The purpose of the segmented source described here is the generation and control of sheared plasma flow for the study of inhomogeneity on the excitation and propagation of electrostatic plasma waves.

The plasma source shown in Fig. 1 is a segmented hot plate that, in some ways, is similar to those used by Jassby.[17] The inner two segments of the hot plate are differentially biasable, while the outer segment is chosen to be grounded. A potential difference applied between the inner two segments generates radially localized, radial electric fields and associated radially localized density gradients. This hot plate, in conjunction with meshes, terminating plates, and/or an electron source, is used to generate and control shear in one component of the ion flow, either perpendicular or parallel to the magnetic field, and has been reported previously.[15,16] In this paper, measurements of the ion-velocity-distribution function, made using laser-induced-fluorescence (LIF) diagnostic techniques[4,18] are used to directly characterize the ion drift velocity $\boldsymbol{U}$ and ion temperature T_i generated by this plasma source.

II. EXPERIMENTAL APPROACH

The segmented source described here was developed at Tohoku University, Sendai, Japan.[15] This segmented source consists of a 1.8-cm-diameter tungsten disk (labeled *E1*) surrounded by two concentric tungsten annuli (labeled *E2* and *E3*) with outer diameters of 4.8 and 7.6 cm, respectively. Only the inner two segments are heated by electron bombardment in the experiment reported here. The outer segment remains relatively cold and electrically grounded and thus contributes a negligible quantity of ions and electrons to the

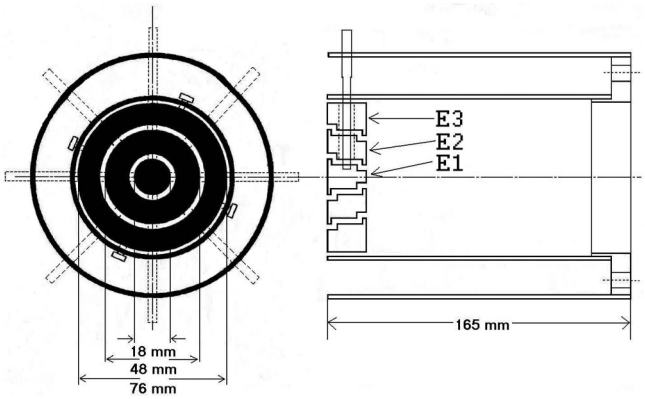

FIG. 1. Scale drawing of segmented source showing segmented hotplate and support structure.

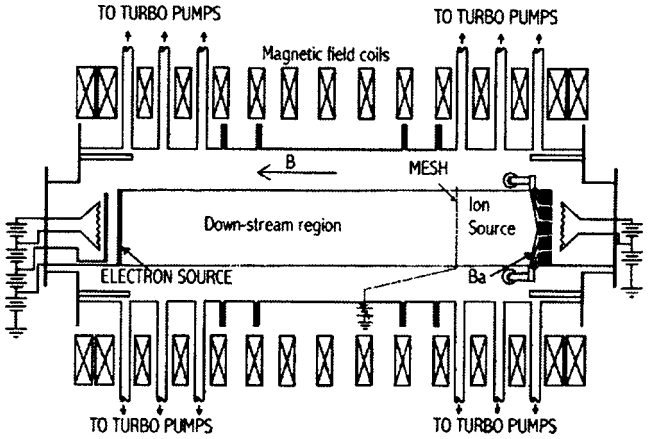

FIG. 2. Experimental setup for the parallel configuration is shown here. The mesh is retracted and the electron source emission is turned off for the perpendicular configuration. The *z* axis is magnetic field aligned with origin at the segmented source.

plasma. All segments are coated with rhenium to increase the work function and, thereby, the contact-ionization probability.[19] The LIF diagnostic techniques used to measure the distribution of alkali ions in both the magnetic-field-aligned (parallel) and perpendicular ion velocity are restricted to barium-ion plasma in the case of the *Q*-machine device.

The segmented source is used in two experimental configurations. The first is called the "perpendicular configuration" for which the segmented source is heated to ~1800 °C and bombarded by barium metal vapor. In this configuration, the segmented source produces both ions (via contact ionization) and electrons (via thermionic emission), while a cold, nonsegmented metal plate terminates the plasma at the other end of the chamber. The inner two segments are set to different bias voltages, resulting in the plasma potential all along the plasma column having an inhomogeneous radial profile determined by magnetic mapping of the segmented source's bias-voltage configuration. In this way, perpendicular-velocity shear is produced by a combination of sheared $E \times B$ flow caused by radially localized, radial electric fields, and diamagnetic plasma flow caused by the associated radially localized density gradients.

In the second configuration, the nonsegmented termination plate is heated sufficiently to exclusively emit electrons (henceforth called the "electron source") and a titanium mesh (8 wires/cm, 0.008 mm wire diameter) is inserted cross sectionally at $z=30$ cm (as measured from the segmented source), as shown in Fig. 2. This electron source is an 8-cm-diameter tungsten disk located 3 m from the ion and electron emitting segmented source. The mesh is biased with $V_{\text{mesh}} \gg k_B T_e/e$ to repel electrons, effectively separating the electric potential in the upstream (segmented-source side of the mesh) and downstream (electron-source side of the mesh) regions as shown in Fig. 3, where k_B is the Boltzmann constant, T_e is the electron temperature, and e is the elementary charge. The electric potential in Fig. 3 is measured with an electrically floating emissive probe,[20] the potential of which deviates from the local space potential by an approximately constant offset (1) due to the unequal electron-collection and electron-emission currents associated with the probe at the space potential, which results in the probe floating potential being more negative than the space potential and (2) due to the heating voltage applied to the probe tip (0.076 mm OD tungsten wire bent in half circle of radius 0.5 mm), an unknown fraction of which contributes to the effective probe bias, resulting in a systematic discrepancy between the potential associated with either end of the emitting filament and the space potential. Although these effects limit the ability to know accurately the space potential at a given point, they do not prevent the electric field (gradient in potential) from being accurately measured.

This method of using a negatively biased mesh to axially separate the electric potential in two regions of magnetized plasma was first used in a study of impurity-driven drift waves[21] (with potassium plasma in one region and cesium plasma in the other region). In that experiment, control over the relative potential difference between the two regions resulted in control over the flux of cesium plasma through the mesh and into the potassium plasma region. In the case of

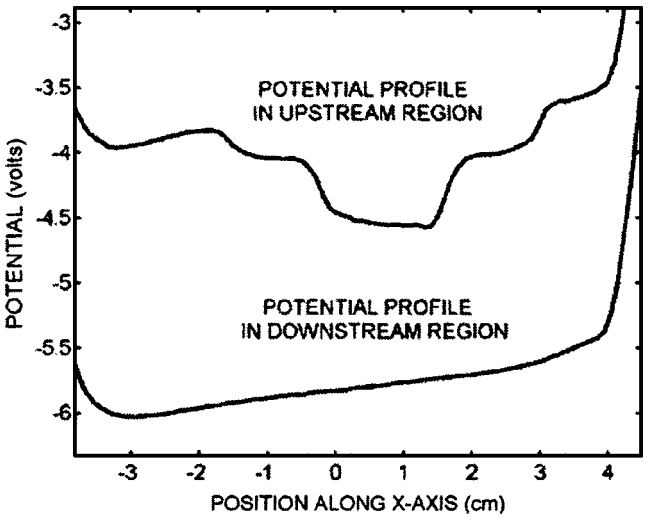

FIG. 3. Floating potential of a floating emissive probe in the upstream (segmented source side of the mesh, $z=15$ cm) and downstream (electron source side of the mesh $z=120$ cm) regions with the mesh biased to -40 V and $B=3.15$ kG. Error bars for these profiles are smaller than the plot lines.

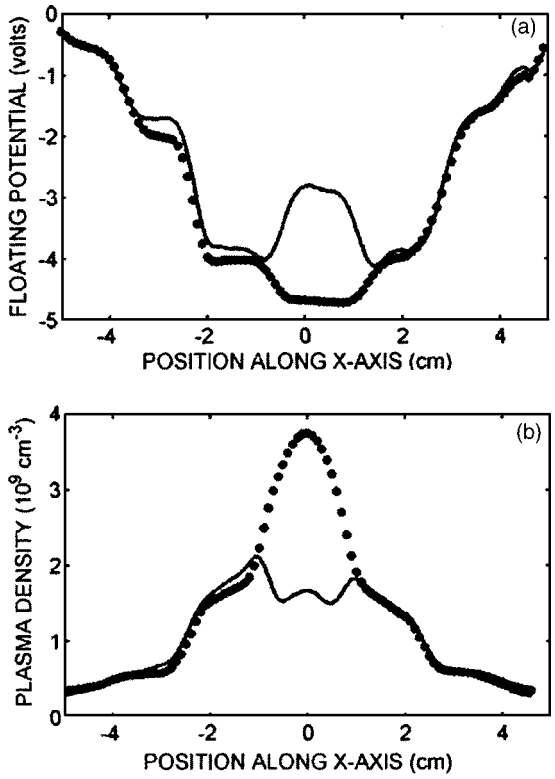

FIG. 4. Radial profiles of potential and density at $z=120$ cm and $B=3.15$ kG. (a) Floating potential of a floating emissive probe and (b) ion saturation current of a Langmuir probe biased to -20 V relative to the floating potential. The second segment is grounded and the inner segment is biased to -0.5 V (1.0 V) for the dotted line (solid line). Error bars for these profiles are smaller than the plot lines.

Fig. 3, the electron source is biased negative relative to the segmented source and consequently the ions experience a drop in plasma potential, and an associated acceleration, as they transit axially through the mesh sheath. As seen in Fig. 3, a nonuniform bias configuration for the segmented source creates structure in the radial profile of plasma potential in the upstream region, whereas the electron source creates a relatively uniform potential profile in the downstream region. As ions transit the mesh sheath, the axial potential drop (ion acceleration) they experience depends on radial position, thus leading to sheared magnetic-field-aligned ion flow (parallel-velocity shear) in the downstream region. Energy analyzer measurements have documented the inhomogeneous radial profiles of ion-parallel-flow energy in the parallel configuration[15] and ion-perpendicular-flow energy in the perpendicular configuration[16] for potassium plasma. Directly documenting the details of the ion-parallel and ion-perpendicular velocity distributions require LIF techniques. This direct documentation is reported here.

III. PERPENDICULAR CONFIGURATION

In Fig. 4(a), the magnetically mapped plasma potential depends on the bias applied to the corresponding segment, making it possible to generate a large (compared to $k_B T_e/e\rho_i$, where ρ_i is the ion Larmor radius) radial electric field at the segment edges. For example, at a magnetic field strength of 2.63 kG and for biases of 2.0 V and 0 V to the segments *E1* and *E2*, respectively, a radial electric field having a radial profile with maximum amplitude of 800 V/m is generated at the segment edges. This radial profile has a half width at half maximum of 3.5 mm, which is comparable to the ion gyroradius of 4 mm. This magnitude is not a limit to the radial electric field obtainable, but it represents a case of large radial electric field for this set of experiments. The localized, radial density-gradient scale-length collocated with this electric field structure is 5 mm. Plasma density profiles are shown in Fig. 4(b) for two center segment bias values corresponding to those shown in Fig. 4(a). It is clear from evaluating $x=0$, $x=\pm 1.5$, and $x=\pm 3.0$ cm in Figs. 4(a) and 4(b) that the plasma density is greatest in regions of lowest plasma potential and that gradients in density are collocated with gradients in potential. In this experiment, the shapes of the electric field profile and the density profile could not be adjusted independently.

The barium ions in this experiment are heavy ($m_i=137$ amu), compared to most other alkali metals used in *Q* machines, and have gyroradii comparable to the half width at half maximum in the radial profiles of potential and density gradients for the range of magnetic field strengths used here, 0.5–3.15 kG. Despite this finite gyroradius, profiles of ion drift U_y at the upper end of this range of magnetic field strength match well with the sum of $E\times B$ and diamagnetic drift velocities calculated using a fluid approximation and the measured local values of electric field and density gradient (i.e., $U_y=-(E_x/B)+(k_B T_{i\perp}/B)(1/n)(dn/dx)$). This good agreement is illustrated in Figs. 5(a) and 5(b), where the ion perpendicular drift profiles are shown for our maximum magnetic field of 3.15 kG and are compared to this fluid model of net drift velocity. The solid line in Fig. 5(a) corresponding to a radially outward electric field, is derived from the solid line in Figs. 4(a) and 4(b). The solid line in Fig. 5(b), corresponding to a radially inward electric field, is derived from the dotted lines in Figs. 4(a) and 4(b). The agreement is less perfect in Fig. 5(b) at $x=\pm 0.8$ cm. The shear is computed for the radially outward electric field case shown in Fig. 5(a) and plotted in Fig. 6. The case of Fig. 5(a) is chosen for further analysis to demonstrate an ion flow profile with large shear at $x=1.3$ cm and solid-body like rotation for $|x|<1.0$ cm. To calculate the shear close to the axis of a cylindrical plasma column, the data must first be transformed into rotation rate[9] Ω_{rot} (shown in Fig. 6 with circles) and then the radial derivative is calculated. The diamonds in Fig. 6 represent the rotational shear ($d\Omega_{rot}/dr$) normalized to Ω_i which has a maximum of $0.46(\pm 0.16)$ cm^{-1} at $r=1.3$ cm. To obtain the normalized velocity shear at this point one need only multiply the normalized rotational shear by the value of radius at that point, which gives a maximum velocity shear for this case of $0.6(\pm 0.2)$ Ω_i.

Measurements of both ion perpendicular and ion parallel velocity distributions indicate that the ion perpendicular temperature is larger than the ion parallel temperature by a factor from 1 to 5. The ion perpendicular temperature increases for increasing radial electric field strength (i.e., increasing potential difference between segments). The causes for this increases in ion temperature are the subject of continued investigation and beyond the scope of this paper. The increase in

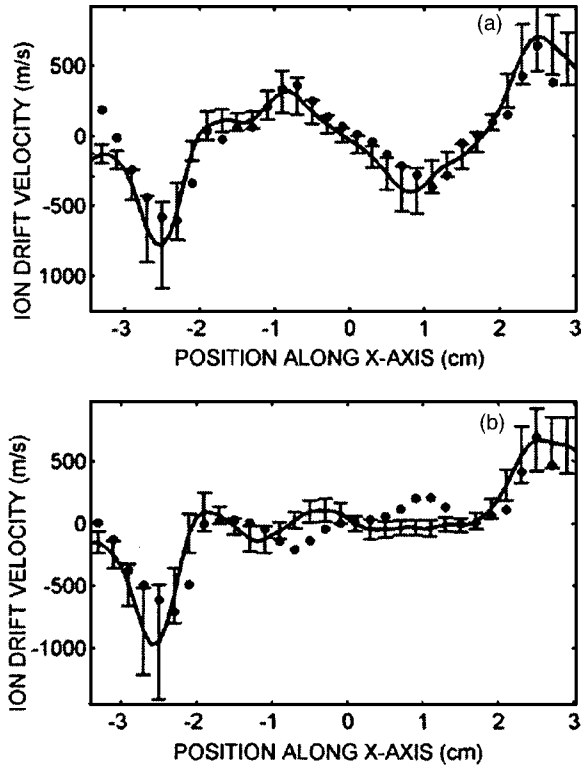

FIG. 5. Radial profiles of ion perpendicular drift velocity at $z=90$ cm and $B=3.15$ kG. (a) case of radially outward electric field (b) case of radially inward electric field. The circles are from LIF measurement, while the solid line is the drift profile obtained from analyzing the density and potential profiles with fluid theory. A representative error bar is shown for the fluid-theory-calculated drift velocity.

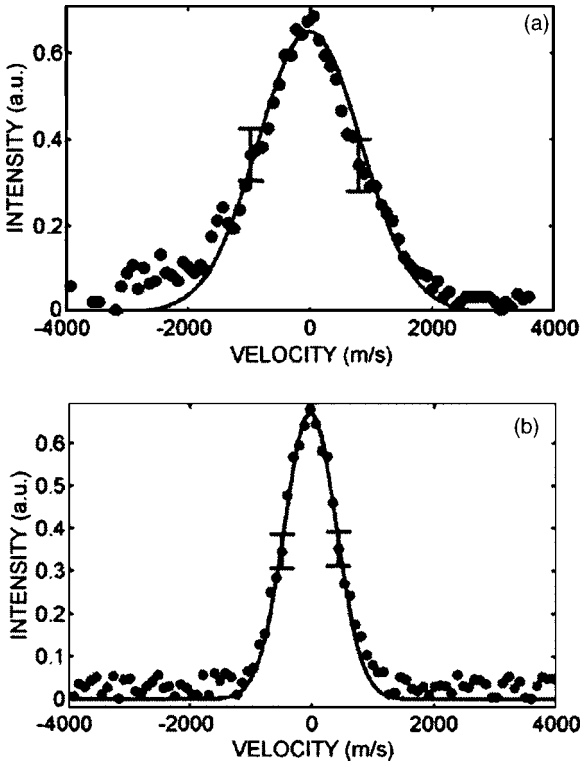

FIG. 7. Comparison of perpendicular and parallel LIF line shapes, measured at $z=90$ cm with $B=2.88$ kG, where the horizontal axis has been converted to ion-velocity relative to the ion frame. (a) perpendicular ion-velocity distribution (b) parallel ion-velocity distribution after subtraction of 0 and 800 m/s average drift velocity, respectively. The solid line in each figure is a representative Gaussian fit to the data. This fit gives $T_{\perp}=1.0$ and $T_{\parallel}=0.24$ eV. Representative error bars are shown.

the perpendicular ion temperature may be related to the work of Sheehan *et al.*,[22] where an increase in the ion-perpendicular kinetic energy density was observed in the wake of a plasma limiter. Ion acceleration by near-wake electric fields was given as a possible cause of the observed energy increase. An example of ion-temperature anisotropy is shown in Figs. 7(a) and 7(b) for the case of 2 V (0 V) applied to *E1* (*E2*). These data are shown in the ion frame (i.e., the average ion drift velocity has been substracted from the parallel velocity data) to allow for convenient comparison of the two line shapes. Fitting a Gaussian to the data gives a perpendicular temperature of 1.0 eV and a parallel temperature of 0.24 eV. The electron temperature T_e (as measured with a swept-bias Langmuir probe) is approximately equal to the ion parallel temperature with $T_e \sim 0.2$ eV, and is insensitive to the potential difference between the segments. Thus, the perpendicular configuration is characterized by ion-temperature anisotropy that is interpreted to be generated by the radial electric fields imposed by the segmented source.

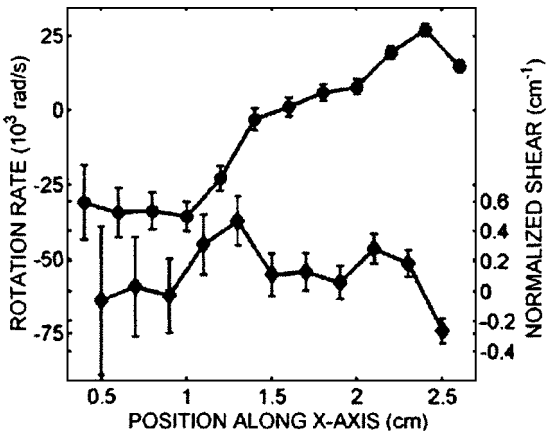

FIG. 6. Plasma rotation rate (circles) and the normalized (to Ω_i) rotational shear (diamonds) for the case of the radially outward electric field shown in Fig. 5(a). This measurement is taken at $z=90$ cm and $B=3.15$ kG.

IV. PARALLEL CONFIGURATION

The measured ion parallel drift U_z velocity at $z=90$ cm and $x=0$ is shown in Fig. 8 as a function of mesh bias for both inner segments grounded and the electron source biased -1.0 V relative to ground. This figure illustrates how separating the upstream and downstream electron populations, due to repulsion by a negatively biased mesh, decouples the radial profiles of plasma potential in the upstream and downstream regions and can lead to an acceleration of the ions as they traverse the sheath potential drop created by the mesh. Figure 9 shows the ion parallel drift velocity at $z=90$ cm and $x=0$ as a function of the difference between the electron-source bias V_{ee} and the center-segment bias V_{ie1} (with mesh biased to $V_{mesh}=-40$ V, $V_{ie2}=V_{ie3}=0$ V). In this case the

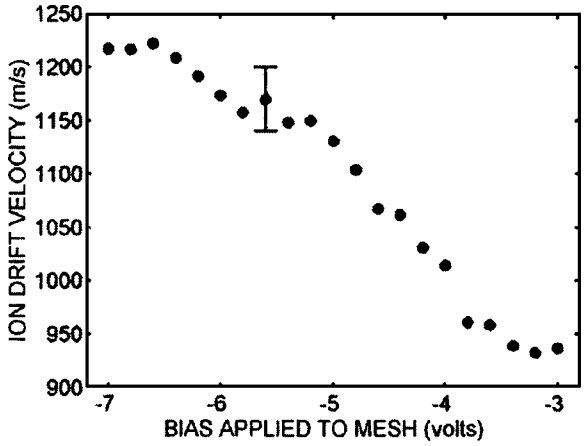

FIG. 8. Ion-parallel drift velocity, measured with LIF at $z=90$ cm and $x=0$, vs mesh bias. For the case of all segments grounded, -1 V on the electron source and $B=1.87$ kG, the ion-parallel drift increases with increasingly negative bias applied to the mesh. The error bar included represents the uncertainty in all data points.

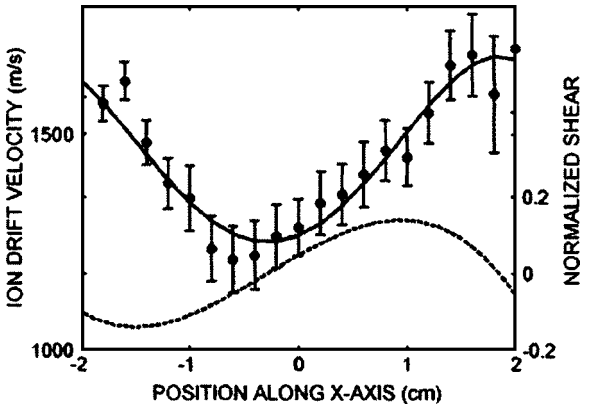

FIG. 10. Ion-parallel drift velocity measured with LIF (circles) at $z=90$ cm and $B=3.15$ kG. The solid line, with a maximum shear of 17% Ω_i, is a polynomial fit to the data, while the dashed line is the derivative (shear) of the polynomial normalized to the ion-cyclotron frequency.

electron-source bias is varied. The ion-parallel drift velocity depends on the value of $(V_{ie1}-V_{ee})$, as expected for ions being accelerated across a potential drop generated by this bias difference. For comparison, the expected drift velocity dependence is also plotted. The expected drift energy $(\frac{1}{2}m_iU_\parallel^2)$ is taken to be the measured drift energy at $V_{ie1}=V_{ee}$ plus the energy gain from a potential drop, due to $\Delta V=V_{ie1}-V_{ee}$, as the ions pass through the mesh.

The electron-source bias, which determines the downstream radial potential profile in the parallel configuration, also influences the downstream density's radial profile since the two profiles are coupled, as demonstrated in Fig. 4. However, the inhomogeneous radial profile of electric potential in the upstream region leads to ion-temperature anisotropy in the upstream region, shown in Fig. 7 for the perpendicular configuration, and this anisotropy carries through to the downstream region. This interpretation of the parallel configuration is consistent with measurements that document the following characteristics: shear in the parallel ion flow, ion-temperature anisotropy, and an absence of both density gradients and radial electric fields.

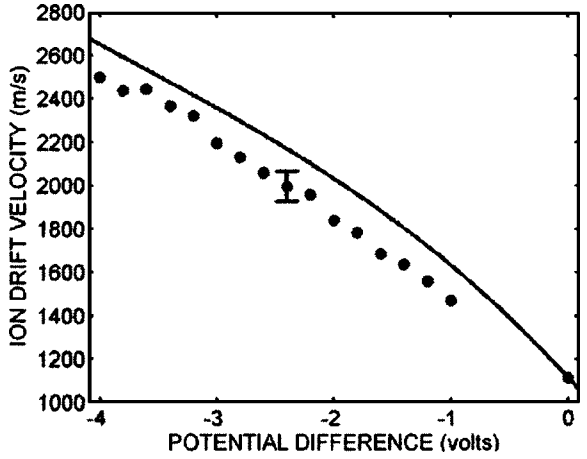

FIG. 9. Ion-parallel drift velocity, measured with LIF at $z=90$ cm, $x=0$, and $B=1.87$ kG, vs the differential bias $(V_{ee}-V_{ie1})$ between the electron source and the center segment. The mesh is biased to -40 V. Circles represent the predicted ion flow based on the energy gain expected from the potential drop. The error bar included represents the uncertainty in all data points.

Control over the potential difference between the inner two segments of the segmented source leads to control over the radial profile of ion-parallel drift velocity U_z. The circles in Fig. 10 show the measured profile for the case where -2.0 V is applied to the center segment, the other segments are grounded, and the electron source is biased to -2.5 V. The solid line in Fig. 10 shows a sheared ion-parallel velocity profile with a maximum shear of $0.17(\pm 0.05)$ Ω_i. It is interesting to note that the ion-parallel flow profile does not have the structure one would expect by assuming it magnetically maps to the segments as the potential profile does. This is understood by taking into account finite gyroradius effects. The ions have a gyroradius of $\rho_i=1.5$–8 mm for $T_{i\perp}=0.2$–1.0 eV and $B=3.15$ kG, which implies that the electron-gyroradius-scale structure generated by the segments is averaged away by gyrating ions, as evidenced by the sharp structure shown in Fig. 4(a) that does not appear in Fig. 10.

V. APPLICATIONS AND LIMITATIONS

The inhomogeneous ion flows and ion-temperature anisotropy producible in the two configurations described here can be applied to the study of waves in the upper ionosphere and magnetosphere where inhomogeneous ion flows and ion-temperature anisotropy often coexist. This segmented source, in the perpendicular configuration, has been applied to investigations of the stability of current-driven electrostatic ion-cyclotron waves influenced by perpendicular-velocity shear localized outside the current channel.[23] There, the waves showed stabilization independent of the sign of the shear. In the parallel configuration, otherwise-stable drift waves arose in the presence of parallel-velocity shear and in the absence of electron current.[24] The characterization reported here has applications to these and more recent investigations[25] of electrostatic waves in sheared ion flows generated by this device. Since the localized electric fields imposed by the

segmented source are coupled with ion-temperature anisotropy and localized density gradients, one cannot adjust the three parameters independently.

VI. CONCLUSIONS

Laser-induced-fluorescence (LIF) diagnostic techniques are used to measure the spatial dependence of the ion-velocity-distribution function of *Q*-machine barium plasma produced on a rhenium-coated, segmented, tungsten hotplate. This source is investigated for two experimental configurations.

The "perpendicular configuration" is characterized by strong, localized, colocated, radial gradients in the plasma potential and density that extend the length of the plasma column. These radial gradients are localized to regions with perpendicular dimension on the order of an ion gyroradius. LIF measurements show that, over most of the radial profile, the azimuthal ion drift compares well with the sum of $E \times B$ and diamagnetic drift velocities calculated in the fluid approximation using the measured profiles of plasma potential and density. Shear in the perpendicular flow profile as large as $0.6(\pm 0.2)\ \Omega_i$ is measured. LIF measurements show that the ion-parallel temperature is insensitive to the strength of the localized radial electric field, while the perpendicular ion temperature increases with increasing radial electric field strength, leading to increasing ion-temperature anisotropy.

The "parallel configuration" is characterized by relatively uniform radial profiles of plasma potential and density on the downstream side of the electron-repelling mesh (compared to the density and potential profiles in the upstream region). The ion-temperature anisotropy in the upstream region carries through to the downstream region. Nonuniform, magnetic-field-aligned ion flow is demonstrated on the electron source side of the mesh. Parallel-velocity shear, as high as $0.17(\pm 0.05)\ \Omega_i$ is measured using LIF in this configuration.

ACKNOWLEDGMENTS

This work was supported by the National Science Foundation Grant No. ATM-0201112, NASA Grant No. NAG5-10218, and Grant-in-Aid for Scientific Research from the Ministry of Education, Culture, Sports, Science and Technology, Japan.

[1] N. Rynn and N. D'Angelo, Rev. Sci. Instrum. **31**, 1326 (1960).
[2] R. W. Motley, *Q Machines* (Academic, New York, 1975).
[3] V. Laul, N. Rynn, and H. Boehmer, Rev. Sci. Instrum. **48**, 1499 (1977).
[4] M. E. Koepke, Phys. Plasmas **9**, 2420 (2002).
[5] N. D'Angelo, Phys. Fluids **8**, 1748 (1965).
[6] G. I. Kent, N. C. Jen, and F. F. Chen, Phys. Fluids **12**, 2140 (1969).
[7] G. Ganguli, Y. C. Lee, and P. Palmadesso, Phys. Fluids **28**, 761 (1985).
[8] G. Ganguli, S. Slinker, V. Gavrishchaka, and W. Scales, Phys. Plasmas **9**, 2321 (2002); V. Gavrishchaka, S. B. Ganguli, and G. Ganguli, Phys. Rev. Lett. **85**, 4285 (2000).
[9] N. D'Angelo and S. von Goeler, Phys. Fluids **9**, 309 (1966).
[10] D. L. Jassby, Phys. Rev. Lett. **25**, 1567 (1970).
[11] J. J. Carroll, M. E. Koepke, W. E. Amatucci, T. E. Sheridan, and M. J. Alport, Rev. Sci. Instrum. **65**, 2991 (1994); M. E. Koepke, W. E. Amatucci, J. J. Carroll III, V. Gavrishchaka, and G. Ganguli, Phys. Plasmas **2**, 2523 (1995).
[12] M. E. Koepke, J. J. Carroll, and M. W. Zintl, Phys. Plasmas **5**, 1671 (1998).
[13] E. Agrimson, N. D'Angelo, and R. Merlino, Phys. Rev. Lett. **86**, 5282 (2001); E. Agrimson, N. D'Angelo, and R. L. Merlino, Phys. Lett. A **293**, 260 (2002).
[14] C. Teodorescu, E. W. Reynolds, and M. E. Koepke, Phys. Rev. Lett. **88**, 185003 (2002); **89**, 105001 (2002).
[15] T. Kaneko, Y. Odaka, E. Tada, and R. Hatakeyama, Rev. Sci. Instrum. **73**, 4218 (2002).
[16] H. Tsunoyama, T. Kaneko, E. Tada, R. Hatakeyama, M. Yoshinuma, A. Ando, M. Inutake, and N. Sato, Trans. Fusion Sci. and Tech. **43**, 186 (2003).
[17] D. L. Jassby, Rev. Sci. Instrum. **42**, 1355 (1971).
[18] D. N. Hill, S. Fornaca, and M. G. Wickham, Rev. Sci. Instrum. **54**, 309 (1983).
[19] P. J. Paris, Rev. Sci. Instrum. **60**, 2802 (1989).
[20] R. F. Kemp and J. M. Sellen, Rev. Sci. Instrum. **37**, 455 (1966).
[21] G. R. Allen, M. Yamada, G. Rewoldt, and W. M. Tang, Phys. Fluids **25**, 2347 (1982).
[22] D. P. Sheehan, J. Bowles, and R. McWilliams, Phys. Plasmas **4**, 3177 (1997).
[23] R. Hatakeyama and T. Kaneko, Phys. Scr., T **T107**, 200 (2004).
[24] T. Kaneko, H. Tsunoyama, and R. Hatakeyama, Phys. Rev. Lett. **90**, 125001 (2003).
[25] T. Kaneko, E. W. Reynolds, R. Hatakeyama, and M. E. Koepke, Bull. Am. Phys. Soc. **49**, 127 (2004); Phys. Plasmas (submitted).